FOI-R--1608--SE
March 2005
ISSN 1650-1942
Technical report

Torleif Martin and Lars M.H. Ulander

FDTD Simulations of the Polarization Dependency of Terrain Vehicles in VHF-band SAR Images

Sensor Technology
SE-581 11 Linköping

SWEDISH DEFENCE RESEARCH AGENCY

Sensor Technology
P.O. Box 1165
SE-581 11 Linköping

FOI-R--1608--SE

March 2005

ISSN 1650-1942

Technical report

Torleif Martin and Lars M.H. Ulander

FDTD Simulations of the Polarization Dependency of Terrain Vehicles in VHF-band SAR Images

Issuing organization	Report number, ISRN	Report type
FOI – Swedish Defence Research Agency Sensor Technology P.O. Box 1165 SE-581 11 Linköping	FOI-R--1608--SE	Technical report
	Research area code 4. C4ISTAR	
	Month year March 2005	**Project no.** E3964
	Sub area code 42 Above water Surveillance, Target acquisition and Reconnaissance	
	Sub area code 2	

Author/s (editor/s)	Project manager
Torleif Martin Lars M.H. Ulander	Lars Ulander
	Approved by Björn Larsson
	Sponsoring agency FMV
	Scientifically and technically responsible Lars Ulander

Report title

FDTD Simulations of the Polarization Dependency of Terrain Vehicles in VHF-band SAR Images

Abstract (not more than 200 words)

The objective of the report is to discuss the relative merits of using HH- or VV-polarization for target detection using synthetic-aperture radar (SAR) in the 20-90 MHz band. The report shows results of computing electromagnetic scattering amplitudes and simulating SAR images of a military terrain vehicle on dielectric ground. Incidence angles studied are 60°, 73° and 85°. The electromagnetic computations are performed using the FDTD method and the SAR simulations are performed using a plane-wave model.

The radar-cross section in the low-frequency limit is generally higher for VV- compared to HH-polarization. This is a consequence of the higher total incident field for VV-polarization. However, the scattering mechanism is more complicated in the studied range of parameters and includes both low- and high-frequency properties.

The main conclusion is that high-frequency mechanisms dominate for incidence angles 60° and 73°, i.e. the scattering comes mainly from the dihedral formed between the vehicle side and the ground. This gives higher radar-cross section for HH-polarization. VV-polarization is slightly higher at the highest incidence angle of 85° due to the angular dependency of the Fresnel reflection coefficients. For foliage-penetration applications, however, it is noted that both forest clutter and attenuation are lower for HH-polarization so that detection performance using HH-polarization will generally be superior to VV-polarization in the studied range of parameters.

Keywords

SAR, FDTD, VHF

Further bibliographic information	Language English
ISSN 1650-1942	**Pages** 26 p.
	Price acc. to pricelist

Utgivare Totalförsvarets Forskningsinstitut - FOI Sensorteknik Box 1165 581 11 Linköping	**Rapportnummer, ISRN** FOI-R--1608--SE	**Klassificering** Teknisk rapport
	Forskningsområde 4. Ledning, informationsteknik och sensorer	
	Månad, år Mars 2005	**Projektnummer** E3964
	Delområde 42 Spaningssensorer	
	Delområde 2	
Författare/redaktör Torleif Martin Lars M.H. Ulander	**Projektledare** Lars Ulander	
	Godkänd av Björn Larsson	
	Uppdragsgivare/kundbeteckning FMV	
	Tekniskt och/eller vetenskapligt ansvarig Lars Ulander	

Rapportens titel (i översättning)

Simuleringar med FDTD av polarisationsberoendet hos terrängbilar i SAR-bilder på VHF-bandet.

Sammanfattning (högst 200 ord)

Målsättningen med rapporten är att diskutera relativa nyttan med att använda HH- eller VV-polarisation för måldetektion med syntetisk aperturradar (SAR) inom bandet 20-90 MHz. Rapporten presenterar resultat från beräkningar av elektromagnetisk spridning och SAR-simuleringar av en terrängbil på dielektrisk mark. Infallsvinklar som studerats är 60°, 73° och 85°. De elektromagnetiska beräkningarna har utförts med FDTD-metoden och SAR-simuleringarna med en planvågsmodell.

Radarmålarean i lågfrekvensgränsen är generellt sett högre för VV- jämfört med HH-polarisation. Detta är en konsekvens av att det totala infallande fältet är större för VV-polarisation. Spridningsmekanismerna inom det studerade parameterintervallet är dock komplicerade och har inslag av både lågfrekvens- och högfrekvensegenskaper.

Den huvudsakliga slutsatsen är att högfrekvensegenskaper dominerar för infallsvinklarna 60° och 73°, dvs spridningen domineras av den dihedral som bildas mellan terrängbilens vertikala sida och marken. Detta resulterar i en högre radarmålarea för HH-polarisation. Vid den största infallsvinkeln 85° så är VV-polarisation något högre p.g.a. vinkelberoendet hos Fresnels reflektionskoefficienter. För tillämpningar avseende vegetationsgenomlysning noteras att klotterspridning och dämpning för HH-polarisation är lägre så att detektionsprestanda generellt sett är bättre jämfört med VV-polarisation inom det studerade parameterintervallet.

Nyckelord

SAR, FDTD, VHF

Övriga bibliografiska uppgifter	**Språk** Engelska
ISSN 1650-1942	**Antal sidor:** 26 s.
Distribution enligt missiv	**Pris: Enligt prislista**

TABLE OF CONTENTS

1. Introduction

Ultra-wideband Synthetic-Aperture Radar (SAR) operating in the VHF band is an active research area with application for detection of vehicle targets concealed under foliage or camouflage. Both Sweden (CARABAS-II [1][2]) and the US (FOPEN SAR [3]) have designed and built airborne technology demonstrators which have shown excellent target detection performance, in particular using change detection in the 20-90 MHz band [4][5]. CARABAS-II has an antenna system with horizontal polarization on transmit and receive (HH-polarization).

The objective of the present work is to investigate whether HH-polarization is optimum or whether vertical-polarization on transmit and receive (VV-polarization) would be expected to improve target detection performance. The size of the studied target is in the same order as the radar wavelength.

The scattering process is illustrated using numerical simulations with the Finite Difference Time Domain (FDTD) method. This method is well suited for ultra-wideband scattering analysis of targets on a homogenous dielectric ground. The targets consist of a military terrain vehicle - also used in [6] - and two vertically oriented plates, which have approximately the same size as the vehicle side and front, respectively. The FDTD program has been developed at FOI [7][12].

2. Scattering analysis

2.1. Incident field near the ground

Since the wavelength of the CARABAS-II radar system varies between 3 meters and 15 meters, a typical target (e.g. a vehicle) will be relatively small compared to the wavelength at lower frequencies and resonant or electrically large at higher frequencies. This is illustrated in Figure 1 where a typical vehicle is shown together with the incident wave, in scale, for the maximum and minimum wavelength of the radar.

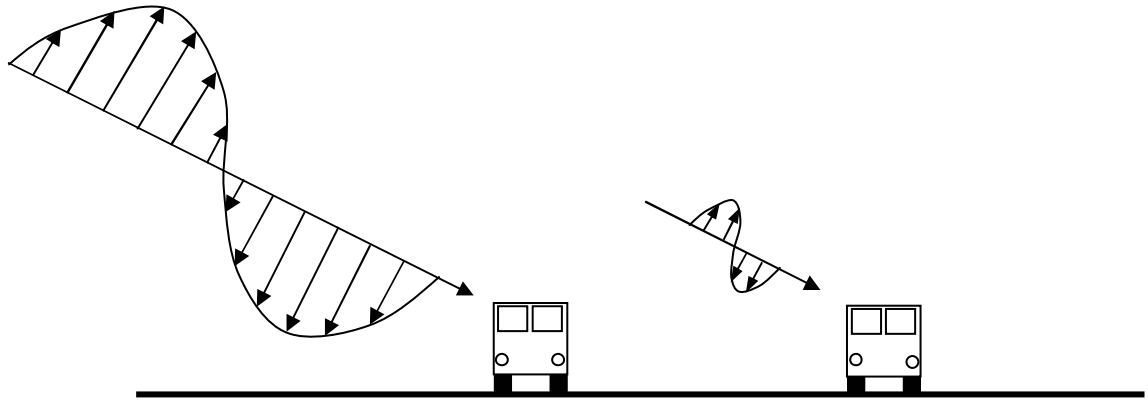

Figure 1. Illustration of radar wavelengths compared to a typical target size (the height of the vehicle is 2.5m). Left: Lower frequency limit, 20 MHz (λ=15m). Right: Upper frequency limit, 90 MHz (λ=3.3m).

The incident electric field at the target will vary as function of frequency, angle of incidence and polarization. The magnitude of the incident electric field at the ground will depend on the polarization, due to the different properties of the ground reflections for each polarization. If we approximate the ground as a homogenous dielectric half space we can use the Fresnel reflection coefficients

$$\Gamma_h = \frac{\cos\theta - \sqrt{n^2 - \sin^2\theta}}{\cos\theta + \sqrt{n^2 - \sin^2\theta}}$$
$$\Gamma_v = \frac{n^2\cos\theta - \sqrt{n^2 - \sin^2\theta}}{n^2\cos\theta + \sqrt{n^2 - \sin^2\theta}} \quad (1)$$

with the vector definitions according to Figure 2. The index of refraction, n, is determined by

$$n = \sqrt{\varepsilon_r + \frac{\sigma}{j\omega\varepsilon_0}} \quad (2)$$

where ε_r and σ is the ground permittivity and conductivity, respectively. The ground parameters used throughout this study are $\varepsilon_r = 10$ and $\sigma = 0.01$ S/m, which are typical values of soil [9].

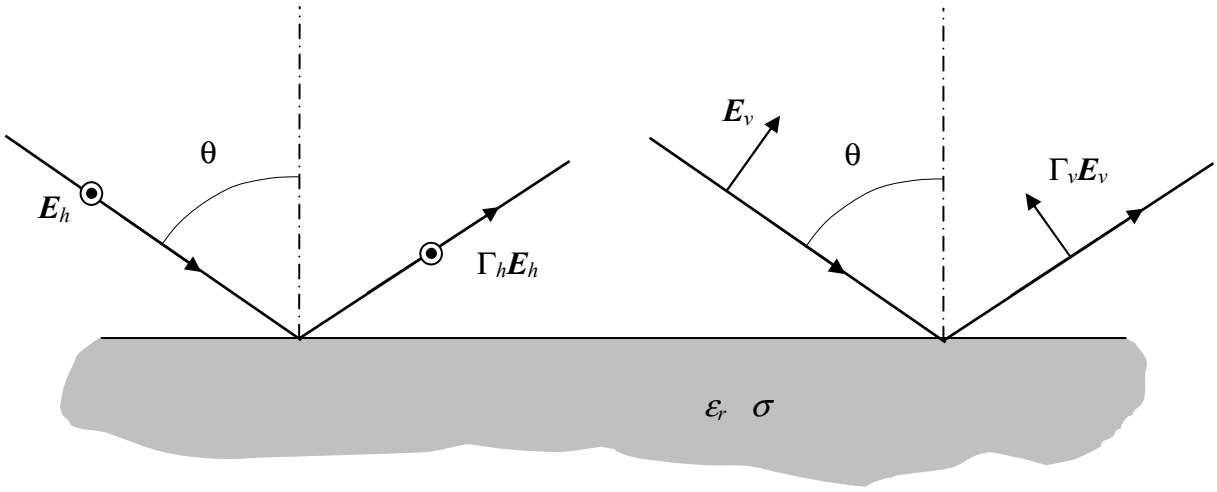

Figure 2. Vector definitions, Left: Incident horizontal electric field. Right: Incident vertical electric field.

The magnitude of the reflection coefficients with these parameters are shown in Figure 3 as function of incident angle for both polarizations for frequencies between 20 MHz and 90 MHz. As illustrated by the plots, the reflection coefficients do not vary much within this frequency band. The coefficient for vertical polarization has a minimum close to $\theta = 73º$, which corresponds to the Brewster angle. At this angle of incidence, most of the field will be refracted into the ground (there is no angle with zero reflection since losses are present in the ground). The phase of the horizontal Fresnel coefficient is close to 180º for all angles in Figure 3. This means that the reflected field has approximately the opposite sign to the incident field. The phase of the vertical Fresnel coefficient is close to 0º up to the Brewster angle where it changes abruptly to nearly 180º. This means that the reflected fields have their signs opposite to the incident fields for *both* polarizations at incident angles larger than the Brewster angle. Hence, the field extinction close to the ground at high incident angles holds for both polarizations (provided that the Brewster angle is exceeded). This will be discussed further in Section 2.4.

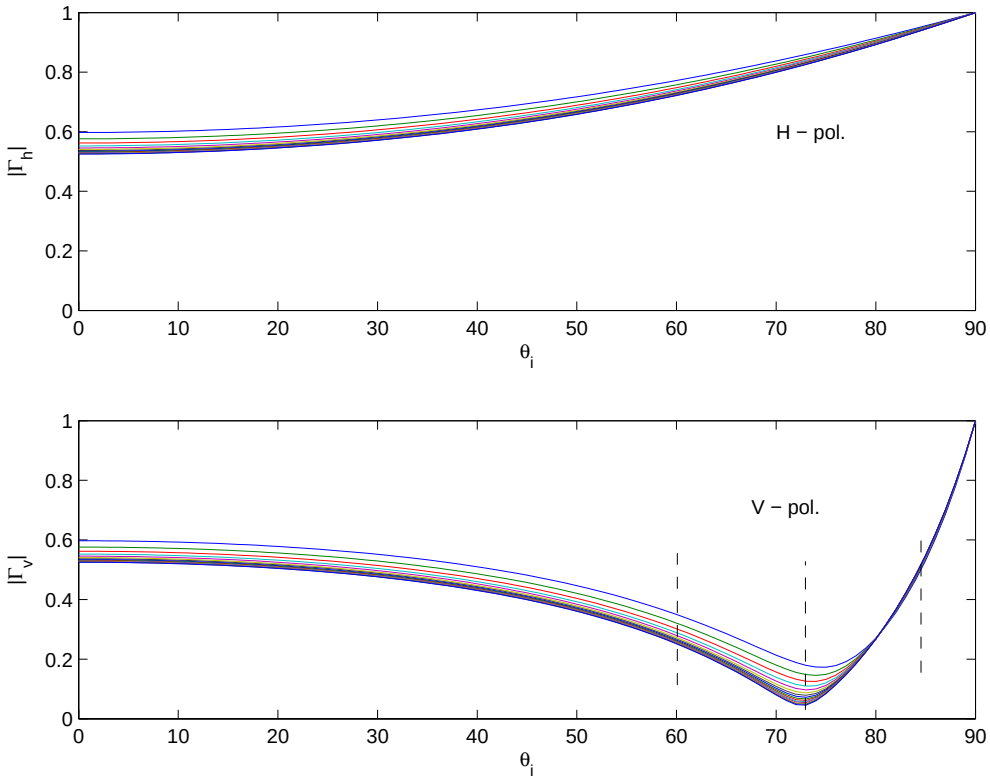

Figure 3. Fresnel reflection coefficients as function of incident angle at 15 different frequencies between 20 MHz and 90 MHz. The vertical dashed lines indicate chosen incident angles for the SAR-images in this study.

Since typical incident angles for the CARABAS-II SAR-system lie in the range 60º - 85º, it is of interest to study the implication of the change in the vertical Fresnel coefficient around the Brewster angle and to compare this with the horizontal case. Three different incident angles have therefore been chosen that lie below, on and above the Brewster angle. These are: $\theta =$ 60º, 73º and 85º, indicated with dashed lines in Figure 3.

A typical target (e.g. a vehicle) often consists of vertical structures, such as the side or front of a truck. It is well known that dihedral scattering between the ground and the vehicle, in many situations dominates the contribution to the SAR image amplitude. By making a simplified analysis of the scattering for a vertical perfectly electrically conducting (PEC) plate, we can identify three different main features of the scattering process, provided that the bandwidth is sufficiently large:

- Low frequency scattering where the object is electrically small.
- Medium or high frequency scattering with small or medium angles of incidence.
- Medium or high frequency scattering with large angles of incidence.

These three cases will be discussed in the following sections.

2.2. Low frequency scattering

At lower frequencies, the currents excited at the object will be related to the incident electric field strength at the object position (scattering of electrically small objects). The field strength

at the ground surface will be dependent on the polarization of the incident field. If we plot the magnitude of the total incident field (incident plus reflected) at the surface level, we get the results according to Figure 4, where we have chosen to show the values as function of incident angle at the middle frequency 55 MHz of the CARABAS-II band.

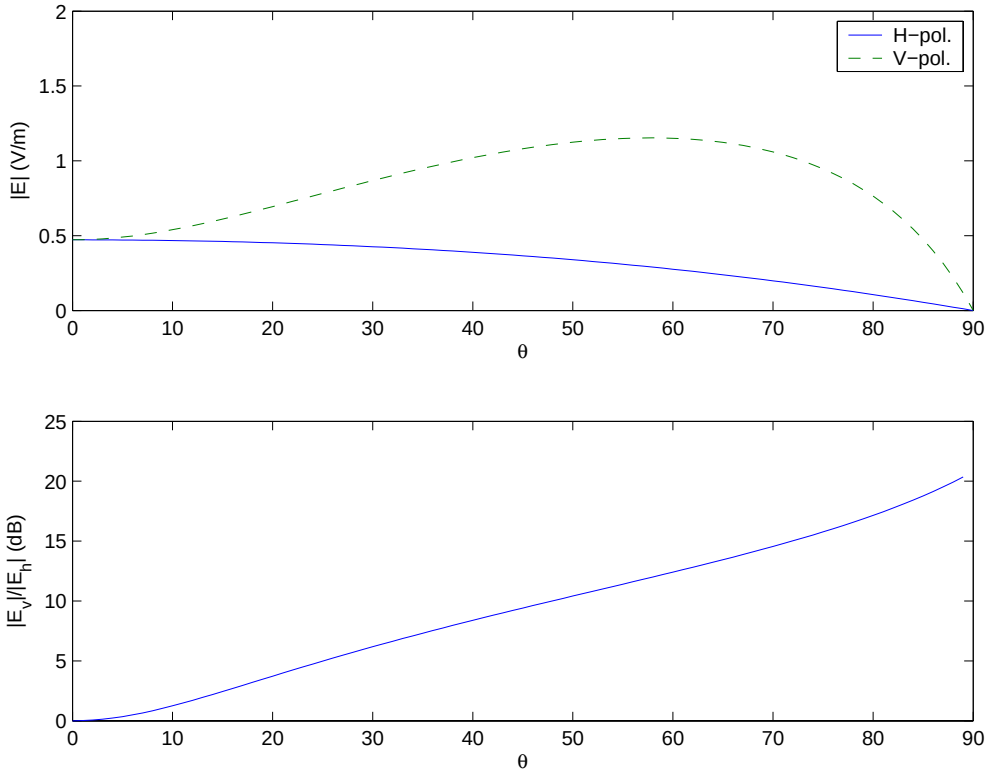

Figure 4. Top: Magnitude of total electric field at the ground surface level at 55 MHz. Bottom: Ratio of electric field magnitudes between vertical and horizontal polarization, at ground surface level. Note that the scale is in dB in the bottom plot.

Due to the different properties of the Fresnel coefficient, the ratio between the vertically and horizontally polarized electric field is large for most incident angles. The largest ratio occurs at high angles of incidence. Electrically small objects that are excited with the field levels shown at top of Figure 4, will obviously scatter the vertically polarized field much more than the horizontally polarized field. This situation holds for small or medium sized vehicles, exemplified with the left drawing in Figure 1.

2.3. High frequency scattering - small and medium incident angles

At higher frequencies, the involved scattering phenomena can to a certain level of approximation be interpreted using high frequency methods, i.e. ray-tracing and physical optics, see Figure 5. Applying a physical optics technique, it is fairly easy to derive an approximate expression for the scattered electric fields from a vertically positioned PEC plate in the monostatic case. If the centre of the plate is positioned at a height h and the area of the plate is A, and further, the height of the plate is H, we can derive the monostatically scattered electric far fields in the direction perpendicular to the plate, as

$$E_h \approx -\frac{jkAe^{-jkr}}{2\pi r}\sin\theta\left[\frac{\sin Z}{Z}\left(1+\Gamma_h^2 e^{-j4kh\cos\theta}\right)+2\Gamma_h e^{-j2kh\cos\theta}\right] \quad (3)$$

$$E_v \approx -\frac{jkAe^{-jkr}}{2\pi r}\sin\theta\left[\frac{\sin Z}{Z}\left(1+\Gamma_v^2 e^{-j4kh\cos\theta}\right)+2\Gamma_v e^{-j2kh\cos\theta}\right] \quad (4)$$

where $Z = kH\cos\theta$. These types of expressions are not sufficiently accurate to use in scattering simulations for SAR images but they can give us a clearer insight of the different phenomena involved in the scattering process. There are three terms within the square brackets in (3) and (4) that corresponds to the three different cases A, B and C in Figure 5.

For low and medium angles of incidence, the sin$Z$/Z -parts in (3) and (4) will be small due to the $\cos\theta$ -factor in Z. These parts corresponds to A and B in Figure 5. The remaining part, proportional to Γ_h and Γ_v in (3) and (4), respectively, is the dihedral scattering event which will be dominating. This corresponds to case C in Figure 5.

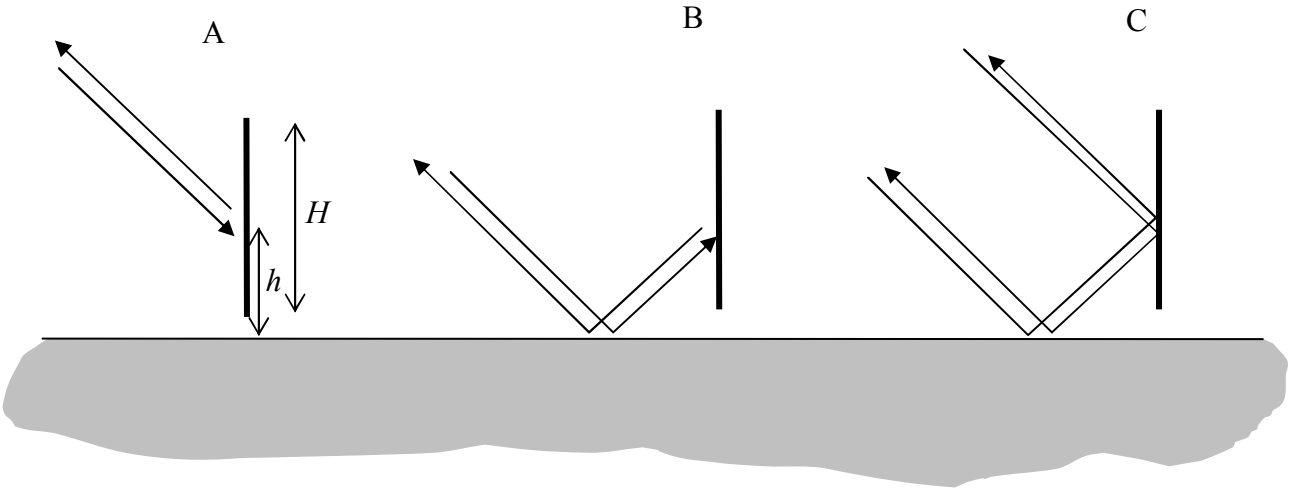

Figure 5. Schematic view of high frequency scattering at a vertical plane. A: Direct scattering from object. B: Scattering with double reflections. C: Dihedral scattering (both ways).

Hence, in this case the scattered field will approximately be proportional to the magnitude of the reflection coefficient. This means that we can expect a higher scattered field for horizontal polarization due to the larger value of the horizontal Fresnel coefficient according to Figure 3.

2.4. High frequency scattering - large incident angles

At higher angles of incidence, e.g. θ=85º, the phase factors depending on $\cos\theta$ and the sin$Z$/Z-factors in (3) and (4) will be close to one, meaning that all three scattering types in Figure 5 will be involved. Also, since the sign of both reflection coefficients are negative (or the phase

is close to 180º) above the Brewster angle, we can approximate the scattered fields for both polarizations as

$$E_{h,v}^{\theta \to 90^o} \approx -\frac{jkAe^{-jkr}}{2\pi r}\left(1-\left|\Gamma_{h,v}\right|\right)^2 \tag{5}$$

This means that the scattered field strength for large incidence angles depends on the difference between one and the magnitude of the reflection coefficient. Since the magnitude of the vertical Fresnel coefficient is smaller than the horizontal Fresnel coefficient (see Figure 3), we can expect a larger high frequency response for vertical polarization as θ gets closer to 90º.

3. Simulation results

3.1. Scattering scenarios

Two similar simulation scenarios were chosen in order to investigate the different scattering mechanisms for horizontal and vertical polarization, see Figure 6. The first is a military terrain vehicle with circular flight tracks along the vehicle side and front. The second is a simplification of the vehicle by using metallic plates with approximately the same size as the vehicle side and front. The dihedral scattering can be studied without complex interaction of different parts of the vehicle in this case. The objects are described in more detail in Section 3.2. The reason for choosing circular flight tracks instead of straight flight tracks is that straight flight tracks imply mixed polarizations of the incident field (if the antenna is fixed on the aircraft) which makes comparisons difficult between the two polarization states.

The aperture angle was 90º for both flight tracks. As mentioned in Section 2.1, three different incident angles were chosen: θ = 60º, 73º and 85º. The minimum number of simulations required along each flight track depends on the object size and the maximum frequency [9].

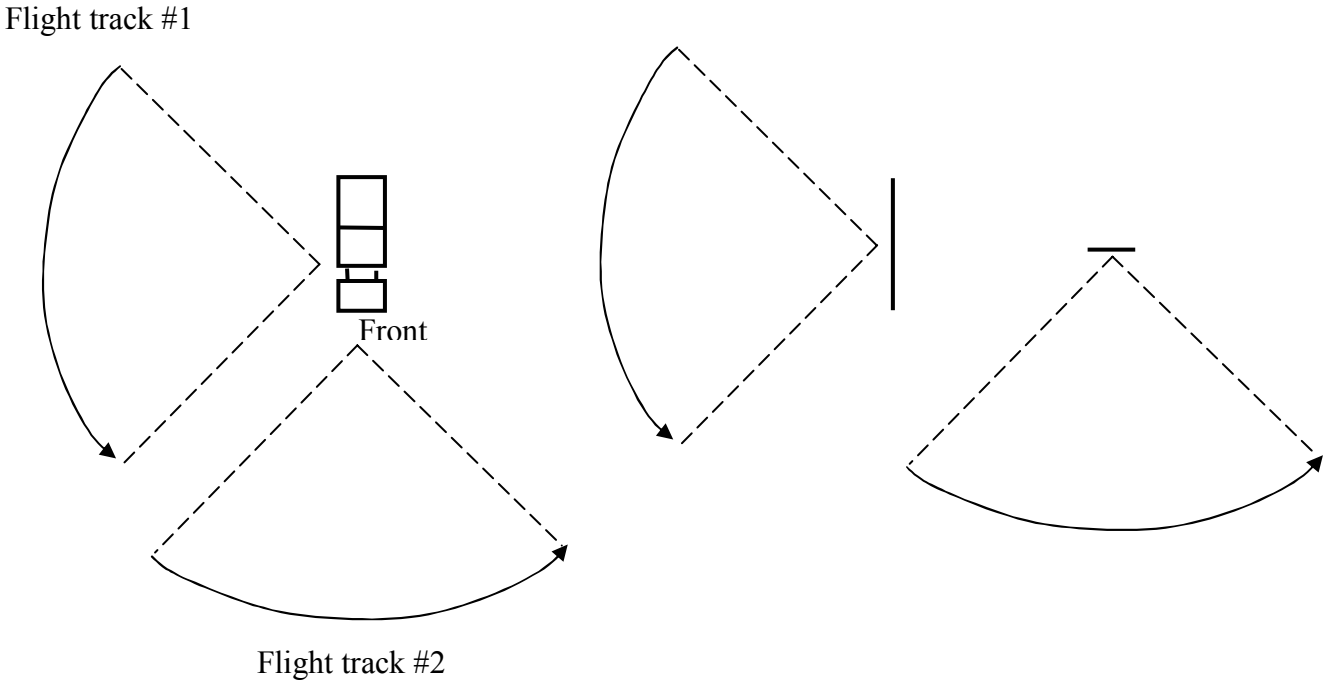

Figure 6. Schematic view of flight tracks and aperture angles for the vehicle and the plates.

3.2. Scattering objects

The first object was a military terrain vehicle (“TGB30”), 6 meters long, 2.4 meters wide and 2.5 meters high. This vehicle geometry was approximated using two vertical PEC plates,

where the first plate is 6m x 2.5m, corresponding to the vehicle side and the second is 2.4m x 2.5m, corresponding to the vehicle front. The FDTD model of these objects is shown in Figures 7 and 8.

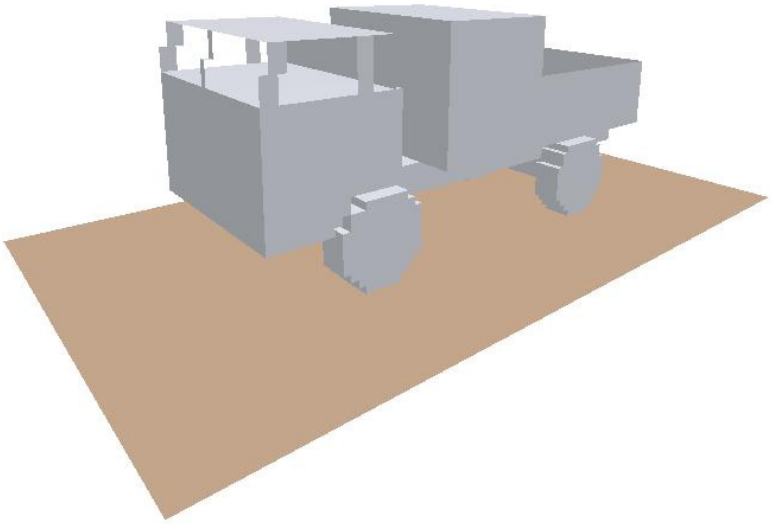

Figure 7. FDTD model of vehicle. The cell size is 10cm cubic.

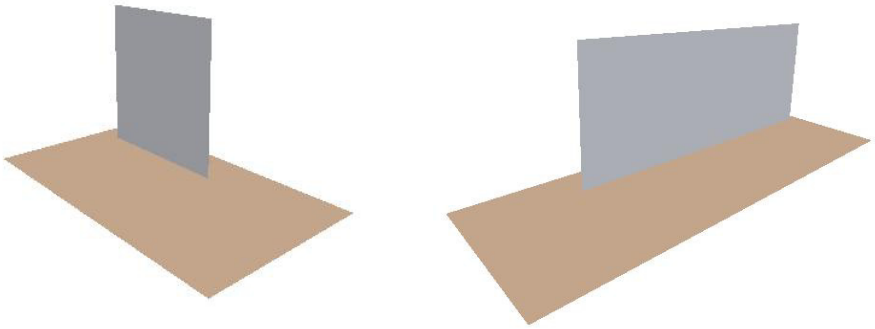

Figure 8. Plates with sizes approximately the same as the vehicle front and side, respectively. The plates are placed 0.5m above the ground.

3.3. SAR images

SAR images were simulated using a simplified image processing technique, which assumes plane wave illumination. This is described more thoroughly in [6]. Figures 9-10, 13-14 and

17-18 show the SAR images (σ^0 in dB) of the vehicle for horizontal and vertical polarization, for θ = 60º, 73º and 85º, respectively. Each figure consists of four color images; upper left is the SAR image for side illumination, below is the corresponding image spectrum, upper right is the SAR image for front illumination and below is the corresponding image spectrum. Figures 11-12, 15-16 and 19-20 show the SAR images of the plates. The layout of these figures follows the same principles as for the vehicle figures.

The color scales in the image spectrum are related to the maximum amplitude of each spectrum. The color scales of the SAR images are scaled with respect to the maximum amplitude of all images (vehicle and plates) with the same incident angle. For θ = 60º, the maximum is 11.0 dB which occurs for horizontal polarization. For θ = 73º, the maximum is 10.5 dB which also occurs for horizontal polarization. For θ = 85º, the maximum is -5.8 dB which occurs for vertical polarization.

The main difference between results for the vehicle and the plates is due to that the vehicle side and front surfaces are disrupted (e.g driver cabin and truck bed) and that the vehicle side has varying height due to the booth on the truck bed. Vehicle structures other than the ones on the illuminated side and front do also contribute to the scattering.

The SAR images for the small plate and the vehicle front are similar in shape. There are larger differences between images of the large plate and the vehicle side due to geometrical differences mentioned above. The maximum amplitude is a few dB higher for the plate than for the vehicle with the exception of θ = 60º, where they are similar. The maximum image amplitudes for the vehicle are given in the Table 1:

Table 1. Maximum SAR image amplitude for vehicle

	Horizontal pol.	Vertical pol.
θ=60º	11 dB	2.3 dB
θ=73º	8 dB	2.8 dB
θ=85º	-9.3 dB	-7.3 dB

As indicated by the results presented in Table 1, image amplitudes are several dB higher for horizontal polarization compared to vertical polarization for θ = 60º and θ = 73º. The opposite holds for θ = 85º. In conclusion, horizontal polarization is to prefer up to very high incident angles. In addition, if the target is concealed by trees, we can expect relatively high scattering and attenuation by trees for vertical polarization at grazing incidence favoring horizontal polarization.

As expected, the main contribution to the image amplitude comes from illumination directions perpendicular to the side and the front of the vehicle (or perpendicular to the plates). This can clearly be seen in the image spectra where the highest amplitudes are found in the middle of the sectors spanned by the flight tracks. Since the scattering at these angles dominates the image spectra, it is feasible to study the radar cross section (RCS) as function of frequency at these angles. By inspection of the RCS-plots we can identify the main scattering mechanisms, discussed in Section 2. This is done in Section 3.4.

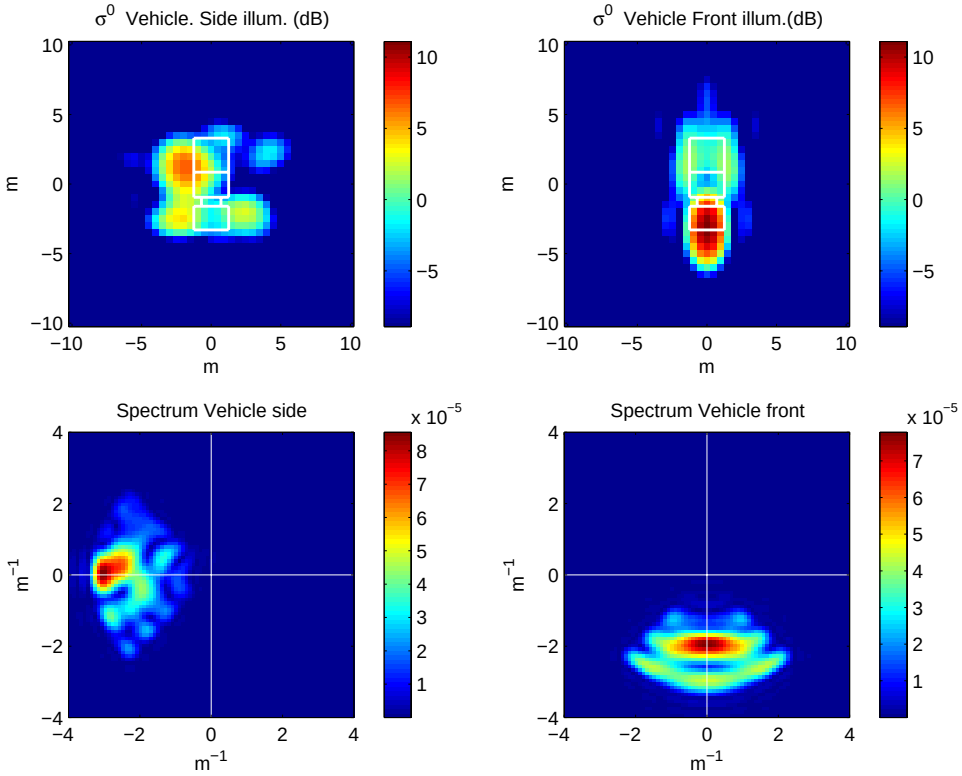

Figure 9. Top: SAR images of vehicle. Horizontal polarization, θ=60°. Side and front illumination. Bottom: image spectra.

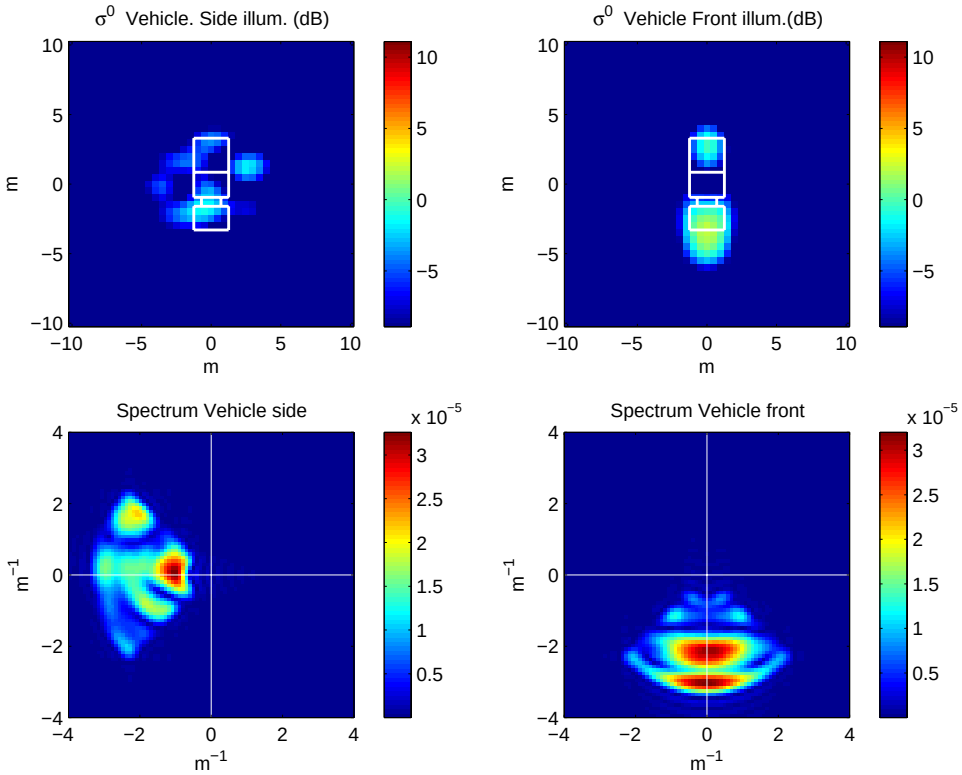

Figure 10. Top: SAR images of vehicle. Vertical polarization, θ=60°. Side and front illumination. Bottom: image spectra.

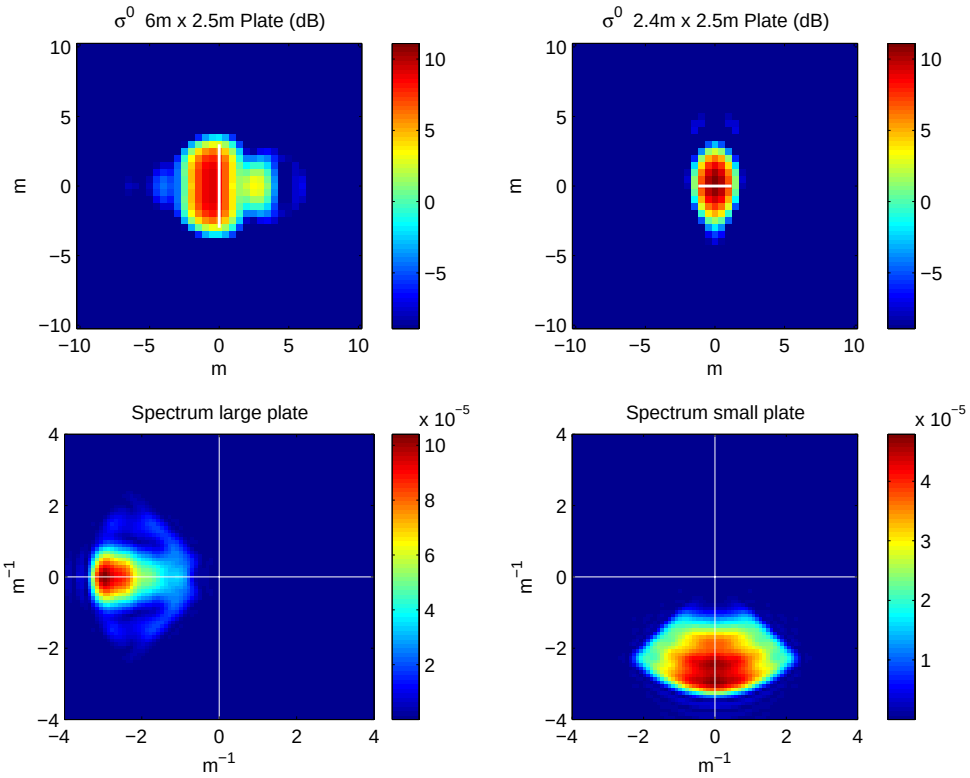

Figure 11. Top: SAR images of plates. Horizontal polarization, θ=60°. Large and small plate. Bottom: image spectra.

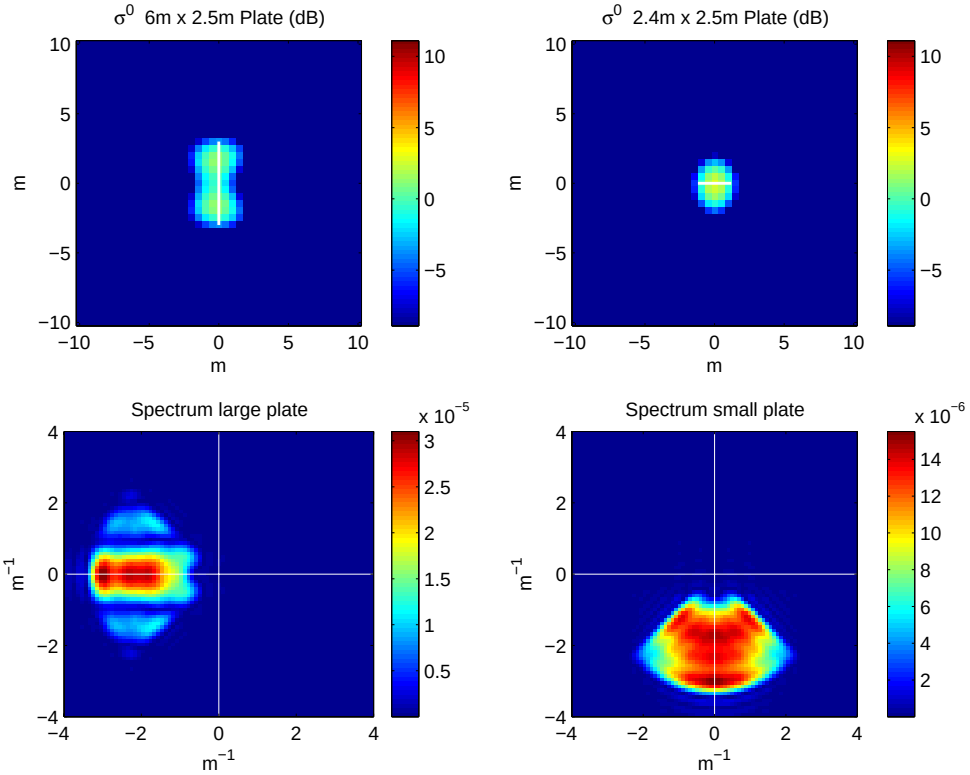

Figure 12. Top: SAR images of plates. Vertical polarization, θ=60°. Large and small plate. Bottom: image spectra.

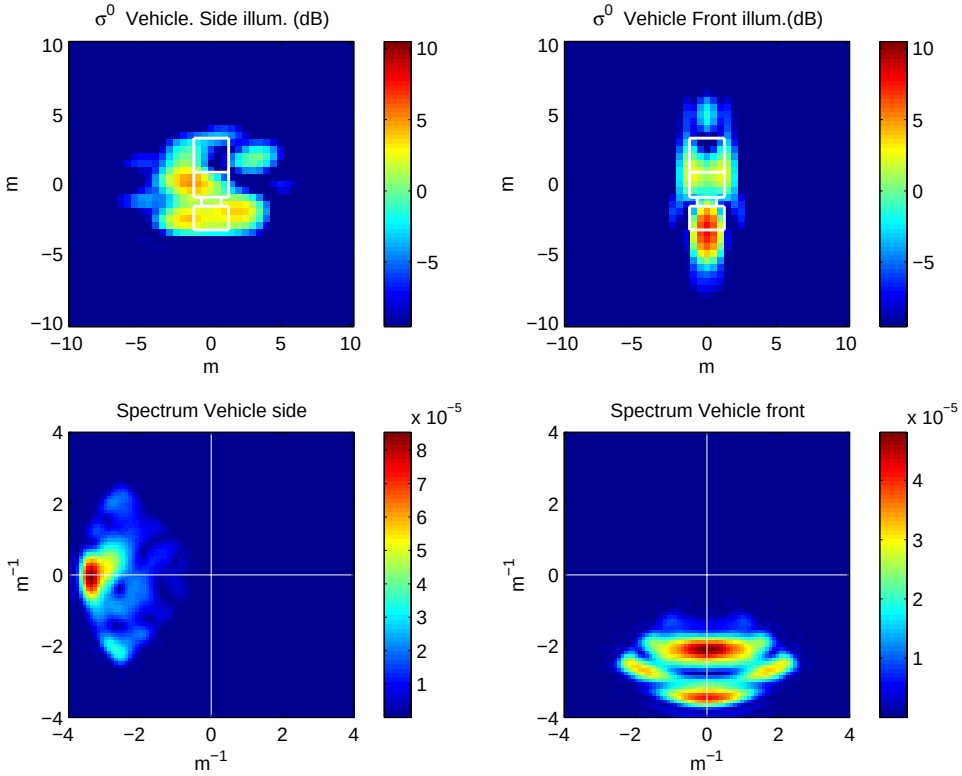

Figure 13. Top: SAR images of vehicle. Horizontal polarization, θ=73°. Side and front illumination. Bottom: image spectra.

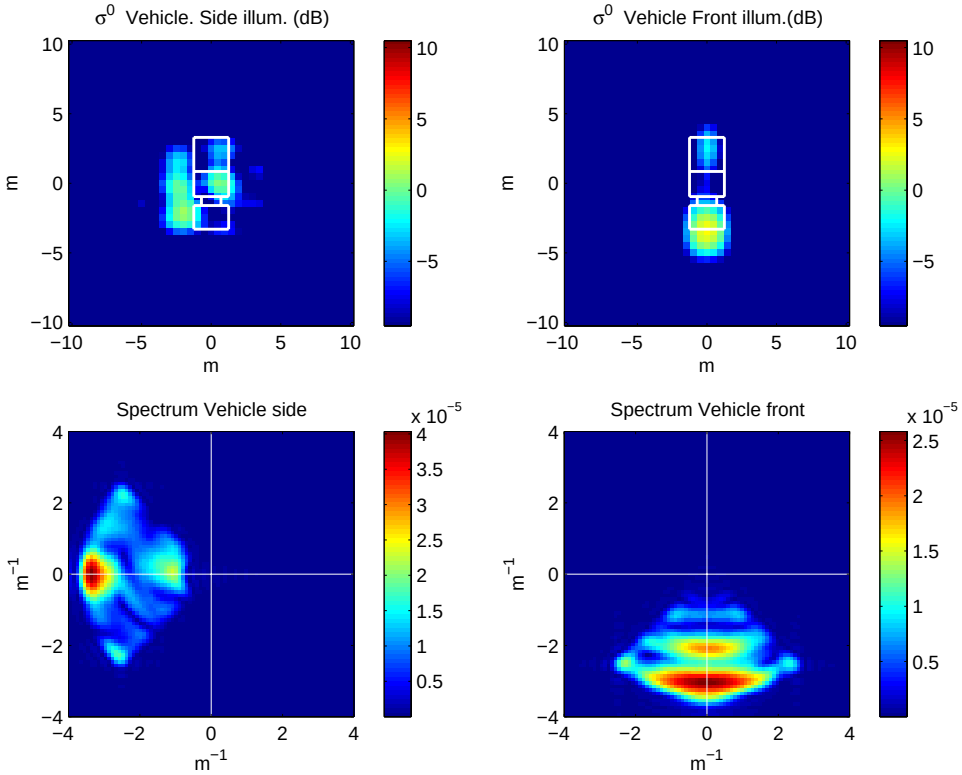

Figure 14. Top: SAR images of vehicle. Vertical polarization, θ=73°. Side and front illumination. Bottom: image spectra.

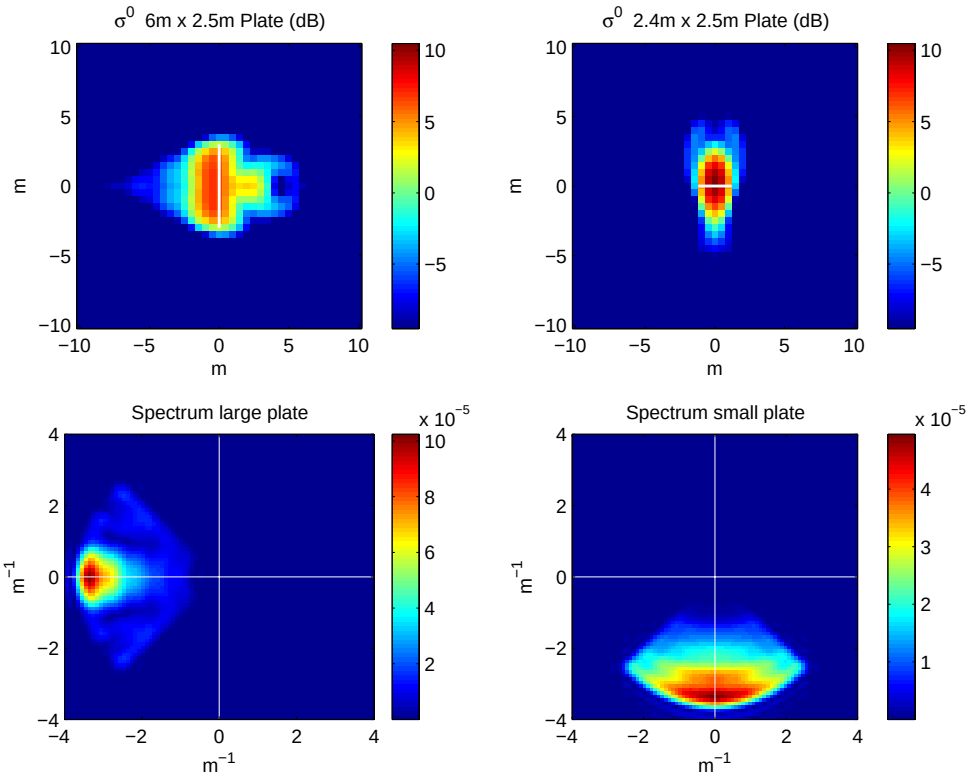

Figure 15. Top: SAR images of plates. Horizontal polarization, $\theta = 73°$. Large and small plate. Bottom: image spectra.

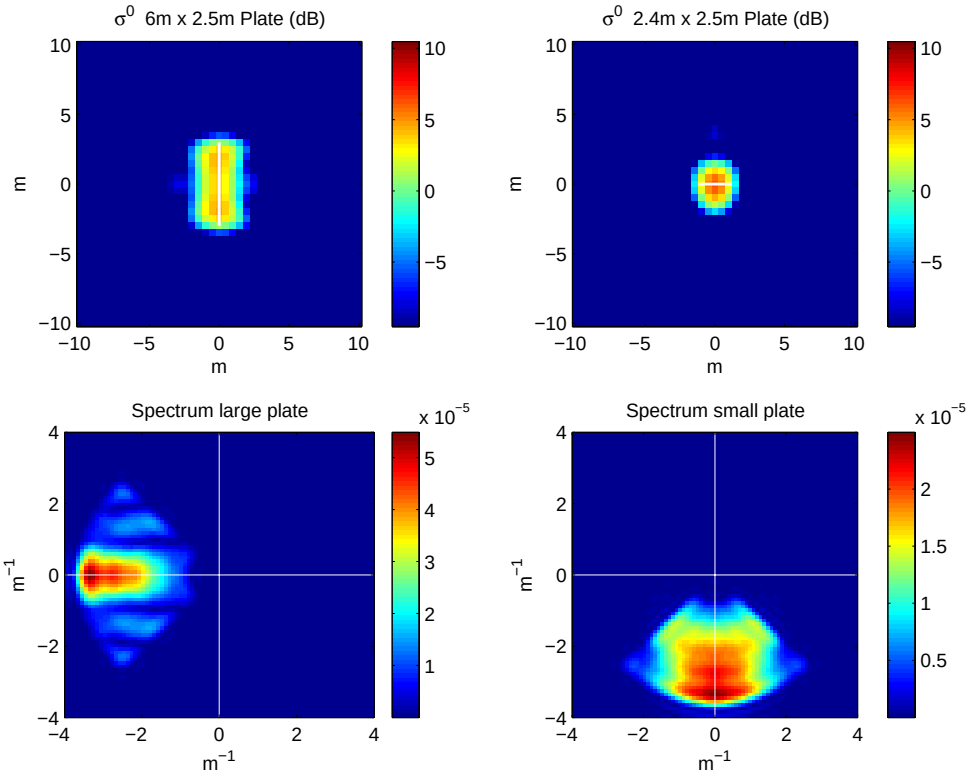

Figure 16. Top: SAR images of plates. Vertical polarization, $\theta = 73°$. Large and small plate. Bottom: image spectra.

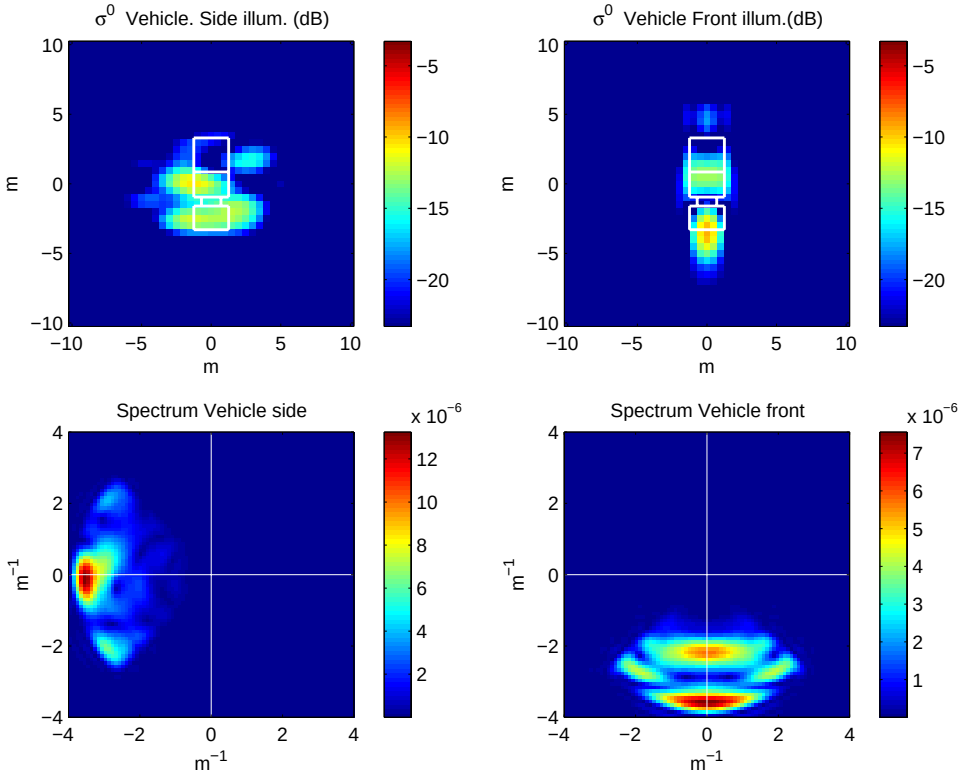

Figure 17. Top: SAR images of vehicle. Horizontal polarization, θ=85°. Side and front illumination. Bottom: image spectra.

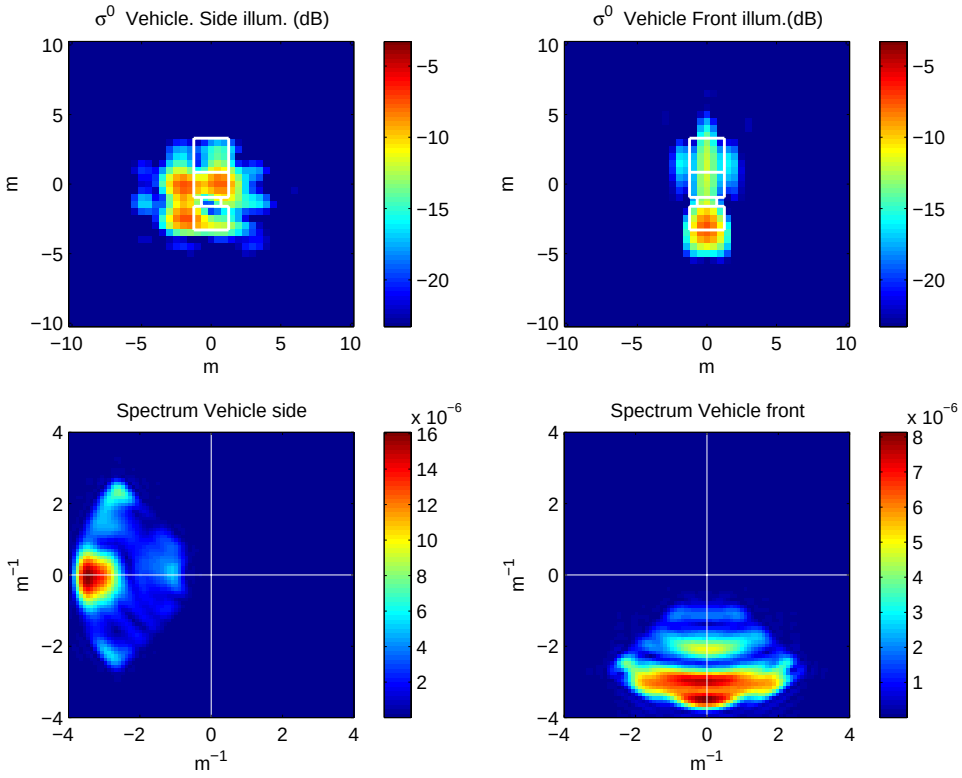

Figure 18. Top: SAR images of vehicle. Vertical polarization, θ=85°. Side and front illumination. Bottom: image spectra.

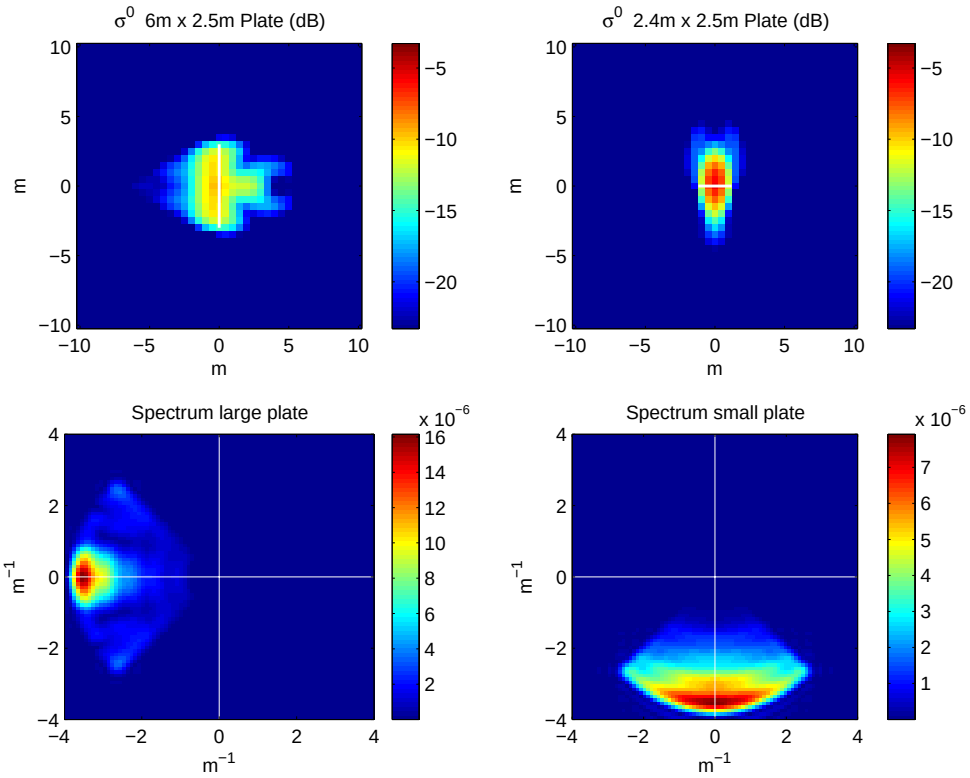

Figure 19. Top: SAR images of plates. Horizontal polarization, θ=85°. Large and small plate. Bottom: image spectra.

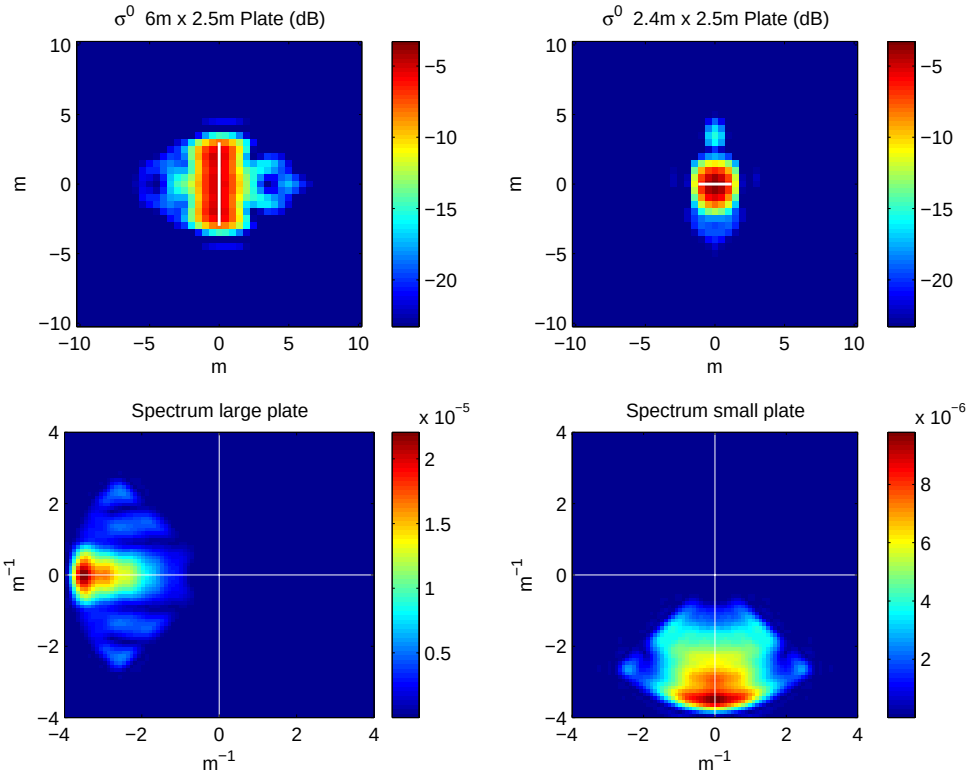

Figure 20. Top: SAR images of plates. Vertical polarization, θ=85°. Large and small plate. Bottom: image spectra.

3.4. RCS plots

The RCS values in the directions perpendicular to the front and side surfaces of the vehicle are plotted together with the RCS of the corresponding plates for both polarizations. The RCS ratio between horizontal and vertical polarization is also plotted below each RCS plot. Figures 21, 23 and 25 show the results for the vehicle side and the large plate. Figures 22, 24 and 26 show the results for the vehicle front and the small plate.

The low frequency scattering effects discussed in Section 2.2 can easily be seen in the figures. The RCS for vertical polarization is generally higher than for horizontal polarization at 20 MHz. An exception can be found for the large plate which has a (dipole-like) half wavelength resonance at approximately 20 MHz. However, the magnitude of the RCS drops dramatically below this resonance (not shown in the plots).

The RCS variations over the frequency band are stronger for the vehicle compared to the plates due to the complexity of the vehicle geometry but the overall correspondence is good with respect to average RCS values.

At higher frequencies we see that the dihedral scattering effect dominates at $\theta = 60^\circ$ and $\theta = 73^\circ$ which gives a higher RCS for horizontal polarization, in agreement with the discussion in Section 2.3. In this case we can expect that the RCS is proportional to the square of the Fresnel coefficient. The ratios between horizontal and vertical polarization are 5 - 10 dB at frequencies where the RCS is high.

Finally, at $\theta = 85^\circ$, we get a slightly higher response for vertical polarization, in agreement with the discussion in Section 2.4. This is due to the dependency on the Fresnel coefficients through (5).

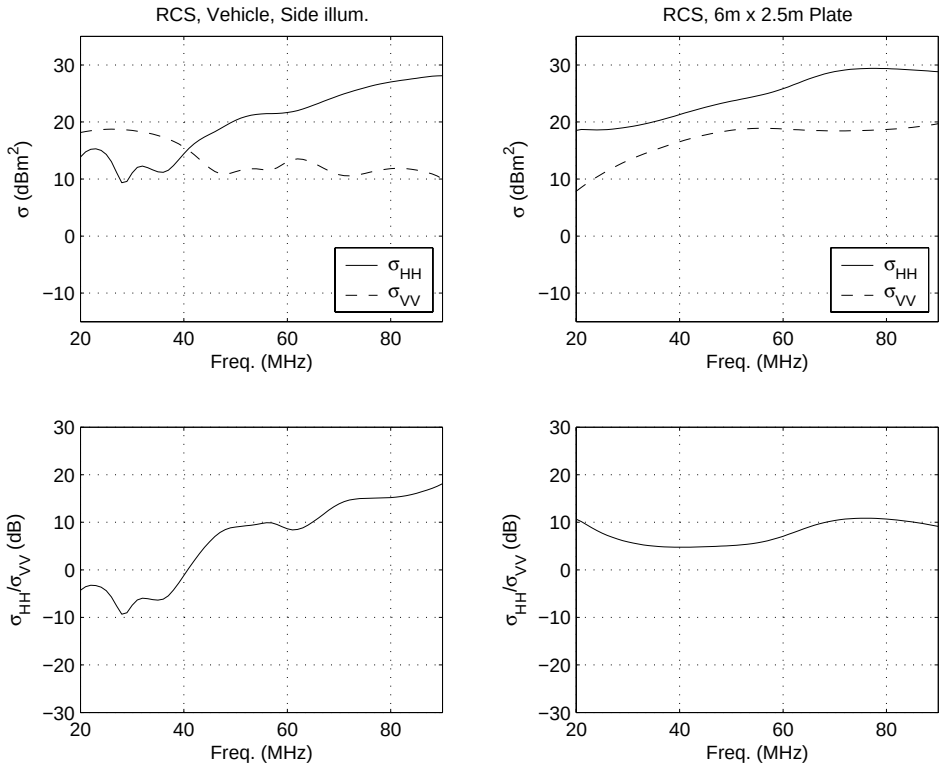

Figure 21. Top: RCS of vehicle (side illumination) and large plate, θ=60°. Bottom: Ratio of horizontal and vertical polarization.

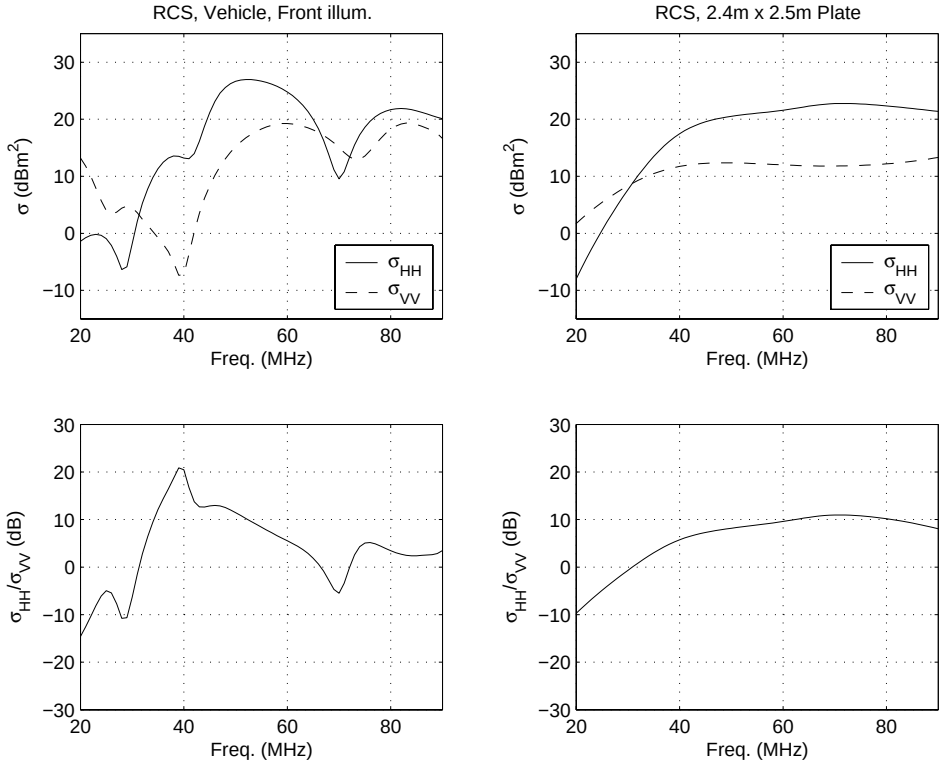

Figure 22. Top: RCS of vehicle (front illumination) and small plate, θ=60°. Bottom: Ratio of horizontal and vertical polarization.

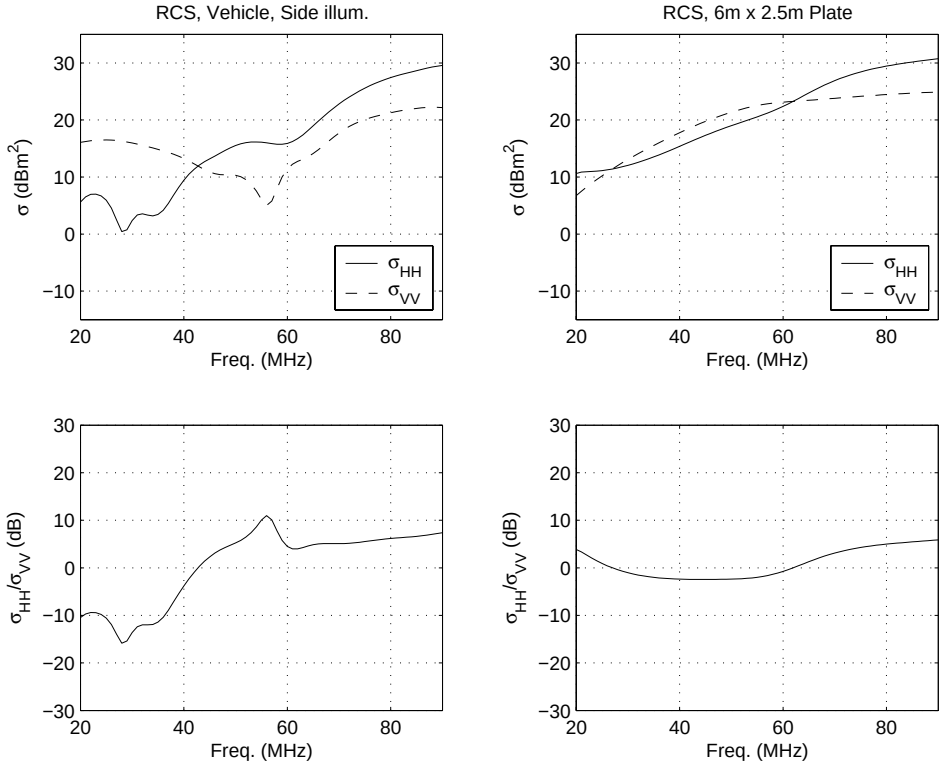

Figure 23. Top: RCS of vehicle (side illumination) and large plate, $\theta = 73°$. Bottom: Ratio of horizontal and vertical polarization.

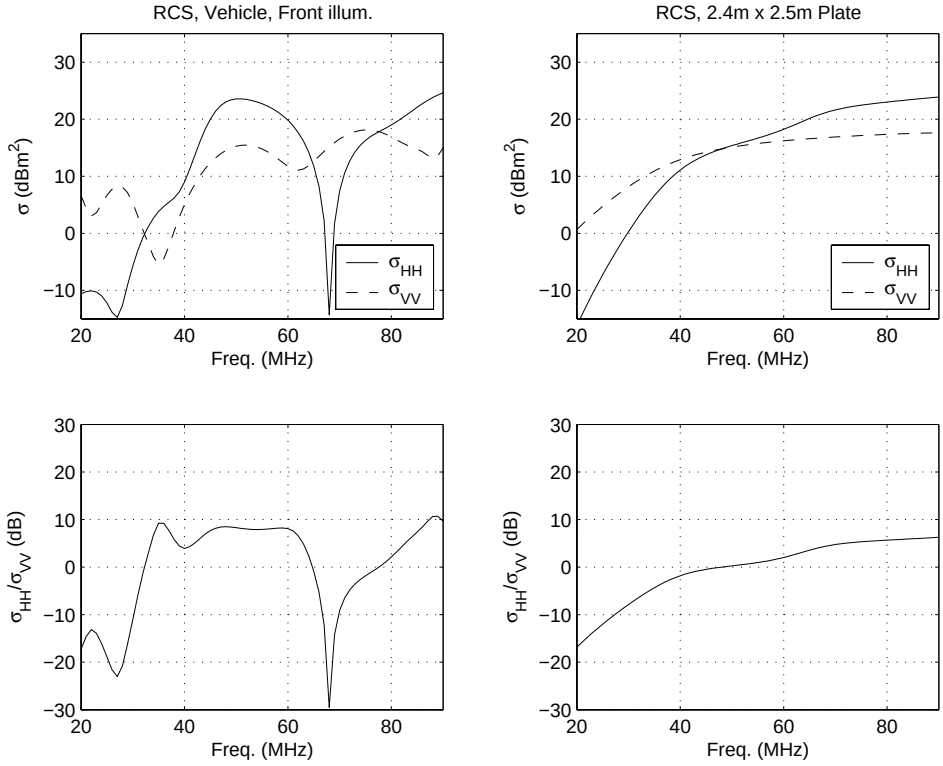

Figure 24. Top: RCS of vehicle (front illumination) and small plate, $\theta = 73°$. Bottom: Ratio of horizontal and vertical polarization.

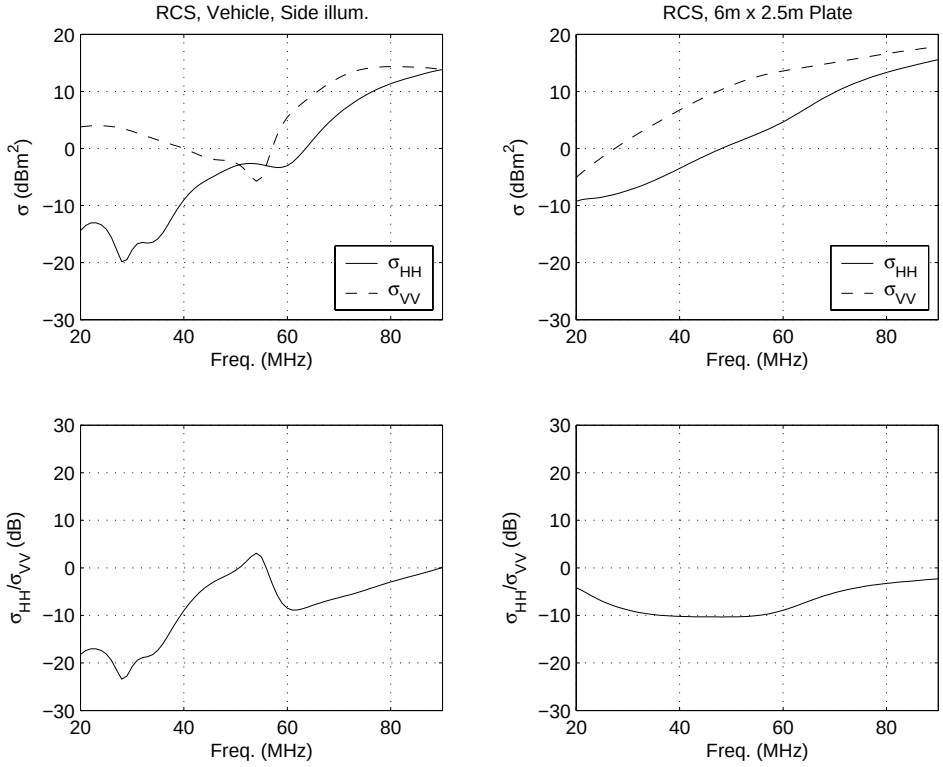

Figure 25. Top: RCS of vehicle (side illumination) and large plate, θ=85°. Bottom: Ratio of horizontal and vertical polarization.

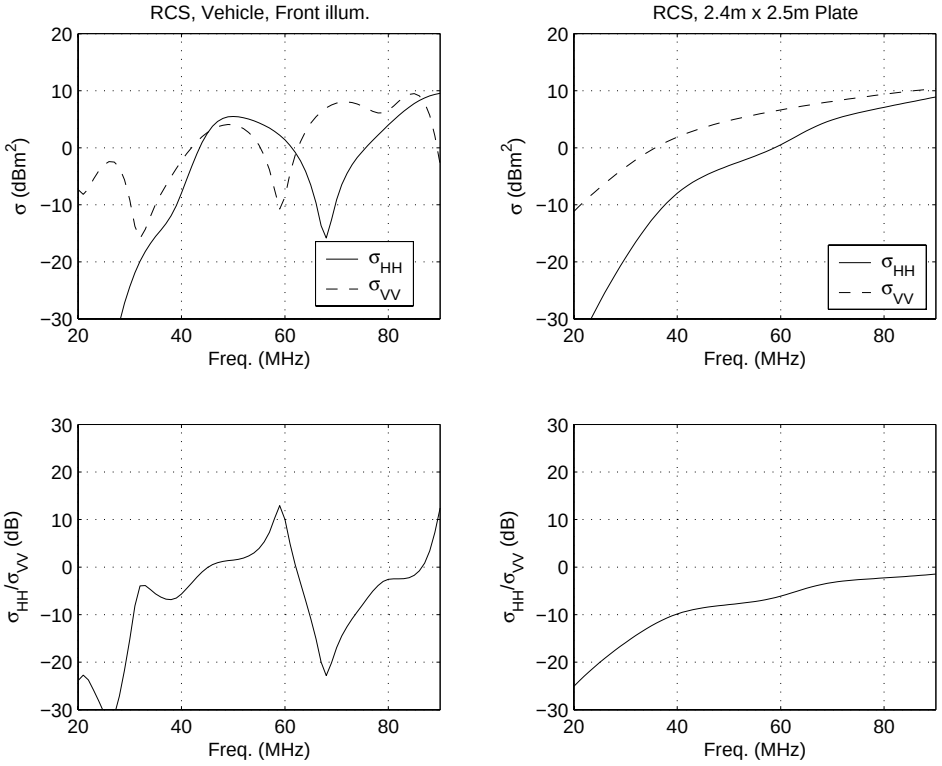

Figure 26. Top: RCS of vehicle (front illumination) and small plate, θ=85°. Bottom: Ratio of horizontal and vertical polarization.

4. Conclusions

The polarization dependency of VHF SAR images has been investigated by FDTD simulations. High-frequency mechanisms dominate for incidence angles of 60° and 73°, i.e. the main scattering comes from the dihedral formed between the vehicle side and the ground. This gives higher radar-cross section for HH-polarization. At the highest incidence angle of 85°, on the other hand, VV-polarization is slightly higher due the angular dependency of the Fresnel reflection coefficients. However, for foliage-penetration applications it is noted that both forest clutter and attenuation is lower for HH-polarization which implies that detection performance using HH-polarization will generally be superior to VV-polarization for the studied range of parameters.

References

[1] H. Hellsten, L.M.H. Ulander, A. Gustavsson, and B. Larsson, "Development of VHF CARABAS-II SAR," in Proc. Radar Sensor Technology, held in Orlando, FL, 8-9 April 1996, SPIE vol. 2747, pp. 48-60, 1996.

[2] H. Hellsten, and L.M.H. Ulander, "The CARABAS II VHF Synthetic Aperture Radar", Chapter 12 in J. Taylor (Ed.), Ultra-Wideband Radar Technology, CRC Press LLC: Boca Raton, pp. 329-342, 2000

[3] J.G. Roos, "Unmasking the Enemy," Armed Forces Journal International, p. 51, April 1998.

[4] L.M.H. Ulander, P.-O. Frölind, A. Gustavsson, H. Hellsten and B. Larsson, "Detection of Concealed Ground Targets in CARABAS SAR Images using Change Detection," Proc. Algorithms for Synthetic Aperture Radar Imagery VI, held in Orlando, FL, 5-9 April, 1999, SPIE vol. 3721, pp. 243-252, 1999.

[5] L.M.H. Ulander, W Pierson, M. Lundberg, and A. Gustavsson, "Performance of VHF-band SAR change detection for wide-area surveillance of concealed ground targets", in Proc. Algorithms for Synthetic Aperture Radar Imagery XI, held in Orlando, FL, 12-15 April 2004, SPIE vol. 5427, pp. 259-270, 2004.

[6] T. Martin, L. M. H. Ulander, "Bistatic SAR Pilot Study: Simulations using FDTD", Report
FOI-R--0839--SE, March 2003.

[7] T. Martin, "An Improved Near- to Far-Zone Transformation for the Finite-Difference Time-Domain Method," IEEE Trans. Antennas Propagat., vol. 46, no. 9, pp. 1263-1271, 1998.

[8] T. Martin and L. Pettersson, "Dispersion Compensation for Huygens' Sources and Far-Zone Transformation in FDTD," IEEE Trans. Antennas Propagat., vol. 48, no. 4, pp. 494-501, 2000.

[9] T. Martin and L. Ulander, "VHF/UHF Synthetic Aperture Radar Image Simulations of a Vehicle using FDTD," Report FOA-R--00-01765-408--SE, 2000.

[10] T. Martin and L. Pettersson, "FDTD Time Domain Near- to Far-Zone Transformation Above a Lossy Dielectric Half-space," ACES Journal, vol. 16, no. 1, pp. 45-52, 2001.

[11] T. Martin, "Broadband Electromagnetic Scattering and Shielding Analysis using the Finite Difference Time Domain Method," PhD thesis No. 669, Linköping University, 2001.

[12] T. Martin and L. Pettersson, "Modified Fresnel Coefficients for Huygens' Sources in FDTD," ACES Journal, vol. 17, no. 1, pp. 30-41, 2002.